

# Gradient enhancement and filament ejection for non-uniform elliptic vortex in 2D turbulence

By Y. KIMURA<sup>1,2</sup> AND J. R. HERRING<sup>2</sup>

<sup>1</sup>Graduate School of Mathematics, Nagoya University, Furo-cho, Chikusa-ku, Nagoya  
464-8602, Japan

<sup>2</sup>National Center for Atmospheric Research, P.O. Box 3000, Boulder, CO 80307, USA

(Received 7 December 2000)

The axisymmetrization of a 2D non-uniform elliptic vortex is studied in terms of the growth of palinstrophy, the squared vorticity gradient. First, it is pointed out that the equation for the palinstrophy growth, if written in terms of the strain rate tensor, has a similar form to that of enstrophy growth in 3D – the vortex-stretching equation. Then palinstrophy production is analyzed particularly for non-uniform elliptic vortices. It is shown analytically and verified numerically that a non-uniform elliptic vortex in general has a quadrupole structure for palinstrophy production, and that in the positive production regions, vortex filament are ejected following the gradient enhancement process for vorticity. Numerical simulations are conducted for two different initial conditions, compact support and Gaussian vorticity distributions. These are characterized by distinctly different features of filament ejection and energy spectra. For both cases, the total palinstrophy production is a good indicator of the development of small-scale vorticity. In particular for the compact support case, a possible intermittency mechanism in the filament ejection process is proposed.

---

## 1. Introduction

Two dimensional turbulence plays a vital role in our understanding of large-scale geophysical flows subject to rapid rotation and stable stratification. As with 3D turbulence, the interplay of *stretching* and *diffusion* is the most essential physical mechanism also in 2D turbulence. The peculiarity for 2D turbulence, however, stems from the fact that “stretching” is NOT associated with vortex lines BUT with vorticity contours. In this paper, we shall consider this interplay and shed new light on it in relation with the gradient enhancement process; a vital nonlinear mechanism of 2D fluid dynamics. The key ingredient on which our analysis focuses is the development of the square of vorticity gradient, the palinstrophy.

The isolated uniform elliptic vortex (the Kirchhoff vortex) continues to attract the attention of many *vorticists*, and indeed to play a fundamental and important role in the study of 2D incompressible flow. The Kirchhoff vortex is a solution of Euler’s equation consisting of a rotating ellipse of axes  $a$  and  $b$  with angular velocity  $\Omega = \omega \frac{ab}{(a+b)^2}$ , where  $\omega$  is the uniform vorticity inside the ellipse. The stability of the Kirchhoff vortex was

first presented for the linear case by Love (1893), who established that Kirchhoff's vortex with an aspect ratio greater than 3 is linearly unstable. †

In contrast to Kirchhoff's vortex, non-uniform elliptic vortex is not an exact solution of Euler, ‡ but still plays an important role in understanding the physics of gradient enhancement and vortex axisymmetrization, both of which are essential ingredients for the mechanism of large scale vortex motion on the earth, including hurricanes. As the pioneering work along this line, we can cite the work by Melander, *et al.* (1987) and subsequently by the group with Zabusky (Yao, Zabusky & Dritschel, 1995; Dritschel & Zabusky, 1996).

Melander *et al.* (1987) concluded that axisymmetrization of an elliptic vortex is implemented by gradient enhancement of vorticity in the core and eventual ejecting vorticity filament outside of it, pointing out that non-uniform elliptic vortex is very unstable compared with Kirchhoff's vortex. The exact stability criterion as far as we know is, however, still an open problem.

We shall show that the above-mentioned mechanism, gradient enhancement and vorticity ejection, can be well interpreted in terms of the palinstrophy and its production. Also palinstrophy production can explain further the micro mechanism which may bridge the two physical concepts in 2D Navier-Stokes turbulence; gradient enhancement and vortex ejection. In particular, it will be shown both analytically and numerically that non-uniform elliptic vortex in general has a quadrupole structure for the palinstrophy production, and that in the positive production regions, vortex filament are ejected following the gradient enhancement process for vorticity. The decay of two dimensional turbulence is, in general, characterized by a cascade of enstrophy (squared vorticity) to ever smaller scales. At sufficiently small scales, viscous dissipation balances the cascade, and the vorticity scale-size distribution declines faster than algebraically. The non-linear aspects of this process conserves enstrophy, with spatial regions of strong cascade identified with positive production of palinstrophy. As the flow evolves, these "cascade" regions comprise a progressively smaller fraction of the space available to the flow. Although the general aspects of the decay is deducible from statistical principles, the question of how intense are regions of palinstrophy production, and their spatial distribution has been entirely deduced from an examination of direct numerical simulations (DNS). The examination of vorticity patterns from such DNS frequently shows elliptical or circular vortex structures. Regions of strong palinstrophy production are seen to be spiral filamentary extrusions from regions of near elliptically organized vorticity. Hence palinstrophy production is a vital element in understanding of the dynamics of enstrophy cascade—particularly its extreme intermittent nature.

The paper is organized as follows. In § 2, we review the theory of the basic equation and palinstrophy production. Numerical results are then presented for two different sets of initial conditions corresponding to cut-off and Gaussian vorticity distributions in § 3, and the discussion and summary are given in § 4.

† The stability analysis for Kirchhoff's vortex was extended by Moore and Saffman (1971) later.

‡ Here by "exact solution" we mean an isolated entity without changing its shape, which does not rule out the possibility of determining the functional form of evolution with respect to time and space.

## 2. Theory

The vorticity equation in two dimensions is

$$\frac{\partial \omega}{\partial t} + (\mathbf{u} \cdot \nabla) \omega = \nu \nabla^2 \omega \quad (2.1)$$

where  $\mathbf{u} = (u, v)$  is velocity and  $\omega = \frac{\partial v}{\partial x} - \frac{\partial u}{\partial y}$  is vorticity and  $\nu$  is kinematic viscosity. Introducing the stream-function  $\psi$  as

$$u = \frac{\partial \psi}{\partial y}, \quad v = -\frac{\partial \psi}{\partial x}, \quad (2.2)$$

we can write the equations in the  $\omega - \psi$  form as

$$\frac{\partial \omega}{\partial t} + J(\omega, \psi) = \nu \nabla^2 \omega \quad (2.3)$$

where  $J(\omega, \psi) = \frac{\partial \omega}{\partial x} \frac{\partial \psi}{\partial y} - \frac{\partial \omega}{\partial y} \frac{\partial \psi}{\partial x}$  is the Jacobian.

From (2.3) we can obtain the following equation for the development of palinstrophy,  $(\partial_t + \mathbf{u} \cdot \nabla)(\omega_x^2 + \omega_y^2) = 2\omega_x \omega_y (\psi_{xx} - \psi_{yy}) + 2\psi_{xy}(\omega_y^2 - \omega_x^2) + 2\nu(\omega_x (\nabla^2 \omega)_x + \omega_y (\nabla^2 \omega)_y)$  (2.4)

where a subscript means the derivative in that direction. Making use of the rate of strain tensor,

$$S = \begin{pmatrix} u_x & \frac{1}{2}(u_y + v_x) \\ \frac{1}{2}(u_y + v_x) & v_y \end{pmatrix} = \begin{pmatrix} \psi_{xy} & \frac{1}{2}(\psi_{yy} - \psi_{xx}) \\ \frac{1}{2}(\psi_{yy} - \psi_{xx}) & -\psi_{xy} \end{pmatrix},$$

equation (2.4) can be rewritten as †

$$\frac{D|\nabla\omega|^2}{Dt} = \underbrace{-2 \frac{\partial \omega}{\partial x_i} \frac{\partial \omega}{\partial x_j} S_{ij}}_{P_s} + \underbrace{2\nu \frac{\partial \omega}{\partial x_i} \frac{\partial (\nabla^2 \omega)}{\partial x_i}}_{P_d} \quad (2.5)$$

It is notable that for 3D turbulence an analogous relation holds for the square of vorticity called enstrophy, namely (Batchelor, 1967)

$$\frac{D|\omega|^2}{Dt} = 2 \omega_i \omega_j S_{ij} + 2\nu \omega_i \nabla^2 \omega_i \quad (2.6)$$

where  $\omega$  is the magnitude of vorticity vector, and  $S_{ij}$  is the rate of strain tensor in 3D. After neglecting the viscous term (and hereafter we will concentrate only on the nonlinear term), equation (2.6) provides all the basics for the analysis of vortex stretching in 3D turbulence. For a summary of research on this topic, see Tsinober(1997). The importance of (2.5) as well as (2.6) is that the Lagrangian dynamics of the magnitude of vorticity and vorticity gradient is described by the components of these quantities and the field data in an Eulerian way. The sign of coefficients or the growth rates of the magnitude if we regard the equations as a self-induction which is deformed by the strain, however, differ in (2.5) and (2.6). The effect of this difference is yet to be known.

To gain some insight into the dynamics of the development of elliptic vortex in general, we assume that the stream function  $\psi$  is of the form,  $\psi(x, y) = F(ax^2 + by^2)$  where  $F$  is an arbitrary (differentiable) function and calculate the functional form of  $P_s$ . Direct substitution gives

† Batchelor (1969) has presented the formula for the volume average of (2.5)

$$\begin{aligned}
P_s &= 64 ab(a-b) xy \times \\
&\quad [-4(F'')^2\{(3a^3x^2 + a^2bx^2 + ab^2y^2 + 3b^3y^2)F'' + 2(a^2x^2 + b^2y^2)^2F'''\} \\
&\quad + F'\{(3a^2 + 10ab + 3b^2)(F'')^2 + 8(a+b)(a^2x^2 + b^2y^2)F''F'''\} \\
&\quad + 4(a^2x^2 + b^2y^2)^2(F''')^2] \\
&\equiv ab(a-b) xy G(x^2, y^2, a, b)
\end{aligned} \tag{2.7}$$

where a prime denotes differentiation with respect to  $z = ax^2 + by^2$ , and the  $G$  is a functional of  $F$ .

From the above, we can observe that :

- [1]  $P_s = 0$  for a circular vortex ( $a = b$ ),
- [2] the  $x$ - and  $y$ - axes are boundaries which separate the regions of the positive and negative palinstrophy production, and discounting a dominant effect from  $G(x^2, y^2, a, b)$ ,  $P_s$  has a quadrupole structure (cf. §4), and
- [3] if we assume that  $ab(a-b)$  has a dominant contribution, under conditions of  $a + b = 1$  and  $a > b$ ,  $P_s$  takes the maximum value at  $a = \frac{3+\sqrt{3}}{6}$ .

We should note that a nonzero  $P_s$  distribution in an isolated vortex does not necessarily mean that the vortex is unsteady. In fact, the Lamb-Batchelor dipole vortex has a symmetric distribution of positive and negative  $P_s$  inside, though it is a steady solution of Euler's equation and propagates without changing its shape. In this case, there should be a subtle balance between enhancement and suppression of vorticity gradient with the steady propagation of the vortex. On the other hand, in 2D turbulence, the normalized volume average of  $P_s$  (the 2D skewness) measures the strength of the cascade of enstrophy to small scales (see *eg* Herring *et al.* 1974).

### 3. Numerical simulation

As the initial vorticity fields, we use two different sets of smooth distributions. One is a compact support and the other is a Gaussian distribution. Both have concentric elliptic equivorticity lines. The assumption of concentric elliptic distribution of vorticity gives a little different testing ground from that for concentric elliptic stream functions which we assumed in the last section. In fact, the former provides similar but a non-concentric elliptic stream function which tend to be more and more circular as the distance from the origin increases. The following numerical simulations will examine some of the predictions made in the last section, and we shall see that the concentric elliptic vortices surely have the quadrupole structure for  $P_s$ .

For integration of the Navier-Stokes equation, the pseudo-spectral method is used with  $2048^2$  grid points and dealiasing by the 2/3-rule. The time marching scheme is a 3rd order Runge-Kutta method with a fixed time step.

#### 3.1. Compact support

As the initial distribution of vorticity we adopt the one used by Melander, *et al.* (1987),

$$\omega(r) = \omega_0 [1 - \exp\{-C \frac{R_0}{r} \exp\left(-\frac{R_0}{R_0 - r}\right)\}] \quad (0 \leq r < R_0) \tag{3.1}$$

where  $r = \sqrt{ax^2 + by^2}$ , and  $\omega(r)$  satisfies  $\omega(r \rightarrow 0) \rightarrow \omega_0$ ,  $\omega(r \rightarrow R_0) \rightarrow 0$ , and we chose  $C = 2.5608517$  so that  $\omega(R_0/2) \sim \omega_0/2$ , and the cut-off radius  $R_0 = \pi/2$ . As the initial

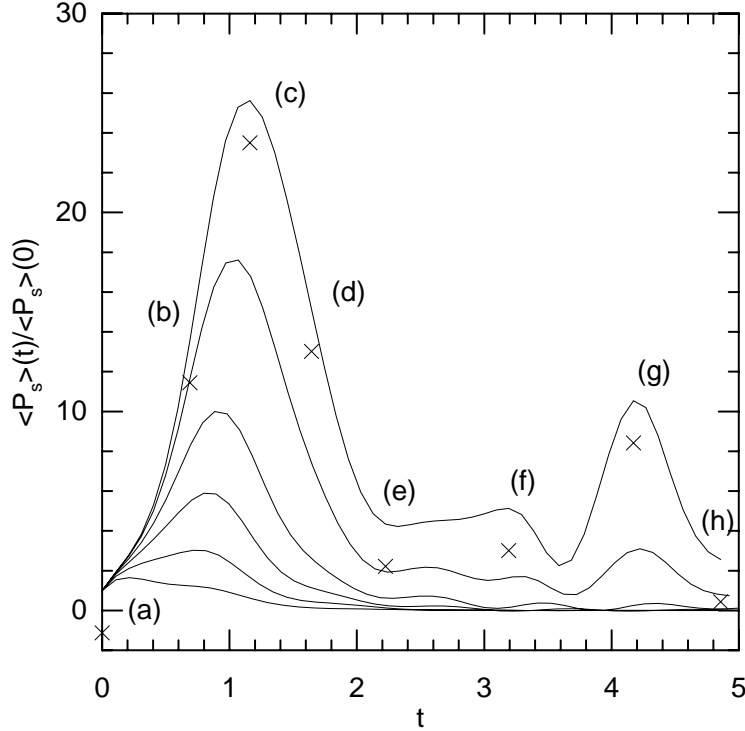


FIGURE 1. The growth of the volume average of the palinstrophy production  $P_s$  in (2.5) for various initial microscale Reynolds numbers in the compact support case. ( $R_\lambda(0) = 2398, 1199, 480, 240, 120, 60$  from the top to the bottom.) The values are normalized by the initial value.

shape of the ellipse we used  $(a, b) = (10, 1)$  which gives the aspect ratio  $\sqrt{10} > 3$ , that is in the unstable regime in terms of the linear stability for Kirchhoff's vortex. Figure 1 is the growth of the volume average of  $P_s$  normalized by the initial value for different initial Reynolds numbers. We see that:

- [1] the initial peak becomes higher for larger Reynolds numbers,
- [2] the curves are oscillatory for all the time range calculated, and the amplitude grows as Reynolds number,
- [3] a secondary peak develops for larger Reynolds numbers.

To see the behavior of the ellipse, we show the sequential snapshots of equivorticity contour lines with the value of  $P_s$  in (2.5) in Figure 2. The sequence is along the curve for the largest Reynolds number in Fig. 1 and the times and values of the total  $P_s$ 's are specified by the cross marks on the curve. In Figure 2, the color code is normalized by a hyperbolic tangent function so that structures with smaller values of  $P_s$  can be seen.

At  $t = 0$  the ellipse is located with the longer axis vertical, which has the quadrupole structure in terms of the palinstrophy production with the x- and y-axes as boundaries just as predicted by the theory in §2 (Fig.2a). In the figure, the 1<sup>st</sup> and 3<sup>rd</sup> quadrants have negative values of  $P_s$  while the 2<sup>nd</sup> and 4<sup>th</sup> quadrants have positive.

As the ellipse rotates anti-clockwise, the contour lines inside get closer in the positive quadrants. At the same time the regions are stretched out and begin to eject vortex filaments, while the negative quadrants are pushed concentrically and contracted (Fig.2b) (equivalent observations were reported in Melander *et. al* (1987) though they didn't use

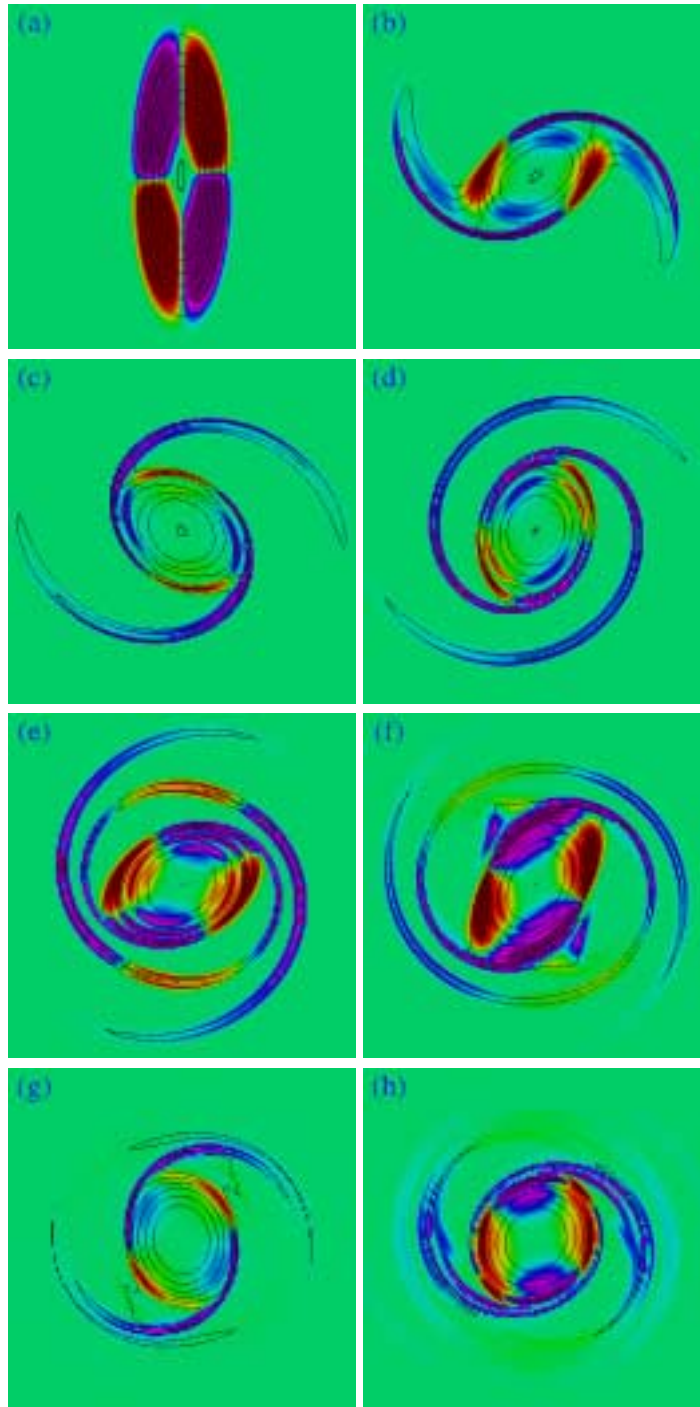


FIGURE 2. Snapshots of the equivorticity contour lines colored with the value of the palinstrophy production for compact support initial conditions. The data are sampled for the highest  $R_\lambda(0)$  case, and the sampling times are indicated by the cross marks with corresponding labels on the plot in Fig. 1.

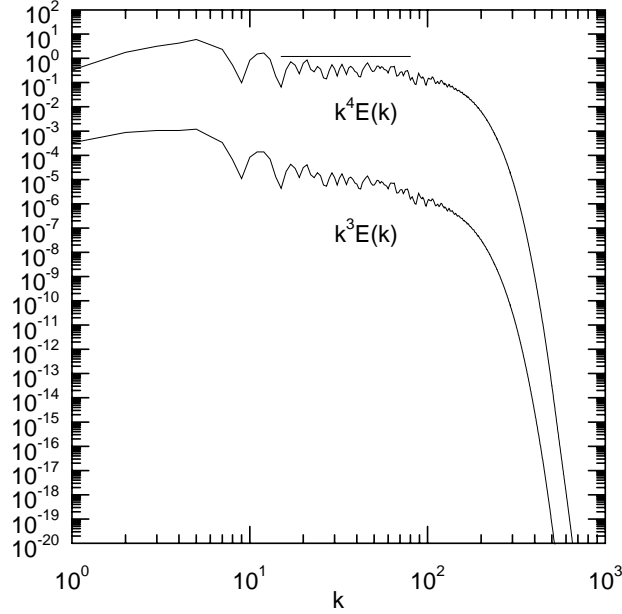


FIGURE 3. The compensated energy spectra,  $k^4 E(k)$  and  $k^3 E(k)$ , for the compact support case at  $t = 4.76$ . The latter is shifted down by 3 decades.

the palinstrophy production and the quadrupole structure of it for their analysis). It is seen that the outer edge of the spirals has a significant positive  $P_s$  value.

The filaments continue to grow, and at the time of the Fig. 2c the total  $P_s$  takes the maximum value and the situation corresponds to the case of the most stretched filaments outside of the vortex core, and we see only small negative  $P_s$  regions mainly concentrates at the edges of the core.

While the core region rotates and gets surrounded by the filaments, the negative  $P_s$  regions grow inside. (Fig. 2d) Then even in the filaments the negative  $P_s$  regions appear (Fig. 2e,f), and eventually the filaments disconnect from the core region. (Fig. 2g) Figure 2g corresponds to the secondary peak of the total  $P_s$  in Figure 1, and the similarity with the state in Fig. 2c can be observed except for the disconnected filaments and the slight change in the core boundary. It seems that the vortex filament ejection for this initial distribution repeats and thus it is in a sense intermittent, and the intermittency can be verified with the plot of total  $P_s$ .

Figure 3 is the energy spectrum at  $t = 4.76$  (close to the time of Fig. 2h). It is compensated by the factor  $k^4$  and  $k^3$  for comparison. (The latter is shifted down by 3 decades.) These factors  $k^4$  and  $k^3$  are from the two distinctive theories on the inertial range spectrum for 2D turbulence; the former by Saffman (1971) which is based on discontinuity of vorticity in the shearing motion of fluids, and the latter by Kraichnan (with a logarithmic correction) (1967) and Batchelor (1969) which assumes enstrophy cascade. The one with the factor  $k^4$  almost levels with fluctuations in particular in the middle range of the wave number,  $20 < k < 70$ .

Figure 4 shows the average of palinstrophy production  $P(P_s | \omega)$  conditionally sampled from the set of equal magnitude of vorticity at the times of Fig.2a to 2g (i.e. at the marked positions in Fig 1.) The figure is plotted as a function of the magnitude of vorticity, and the values are normalized by the maximum value. We observe that the

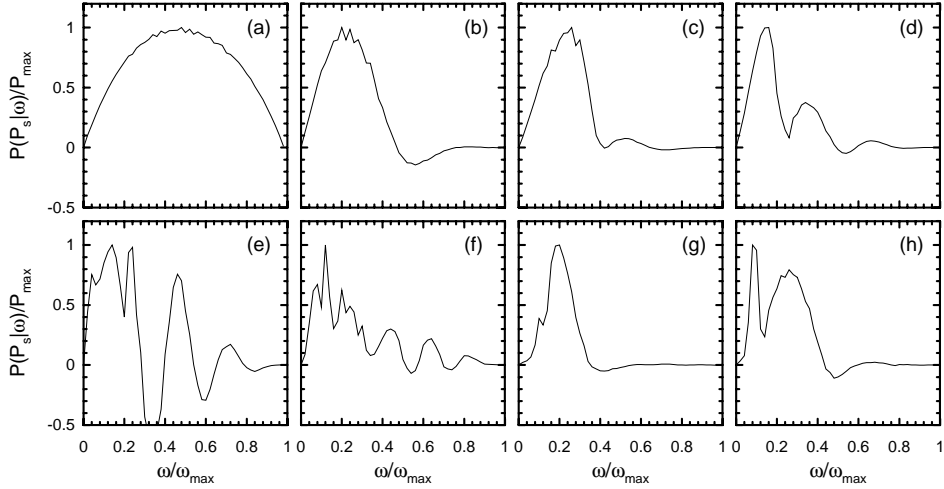


FIGURE 4. Conditional average of the palinstrophy production in terms of the magnitude of vorticity for the compact support case. The labels correspond to those in Fig. 1 and Fig. 2.

palinstrophy production stays almost zero at zero vorticity (back ground) and at the maximum vorticity (core). The core has effectively no palinstrophy production because of cancellation, even though the core contains both strong positive and negative regions.

At  $t = 0$ , the shape of the conditional average is symmetric and the peak is at the middle value of vorticity (Fig. 4a). Until the first peak appears in Fig. 1, the peak shifts to the left (Fig 4b, c). The shift of the peak to the smaller vorticity means that the main contribution to the palinstrophy production comes from the scattered weak vorticity filaments. After passing the first peak in Fig. 1, the conditional average shows rather violent oscillations, but with the major peak being still in the small vorticity region (Fig. 4d,e,f). The oscillation disappears by the time of the second peak in Fig. 1 (Fig. 4g). Again after passing the second peak, we can observe oscillation in particular in the smaller vorticity region. This conditional average of  $P_s$  enables us to verify the intermittency of vortex filament ejection.

### 3.2. Gaussian distribution

As the second type of vorticity distribution, we use the Gaussian distribution,

$$\omega(r) = \omega_0 \exp\{-Cr^2\} \quad (0 \leq r < R_0) \quad (3.2)$$

where  $r = \sqrt{ax^2 + by^2}$  and we chose  $C = 2.8092\dots$  so that  $\omega(R_0/\sqrt{10}) \sim \omega_0/2$ . In this case, the initial micro-scale Reynolds number is similar to the compact support case. The radius is also  $R_0 = \pi/2$ . Hereafter we look at the development of the ellipse in terms of the same issues as before.

Figure 5 is the growth of the volume average of  $P_s$  normalized by the initial value for different initial Reynolds numbers. We see that:

- [1] the initial peak becomes higher for larger Reynolds numbers as before,
- [2] the curves show no oscillation after the peak even for higher Reynolds numbers, and eventually,
- [3] there is no secondary peak.

Figure 6 is the sequential snapshots of equivorticity contour lines colored with the

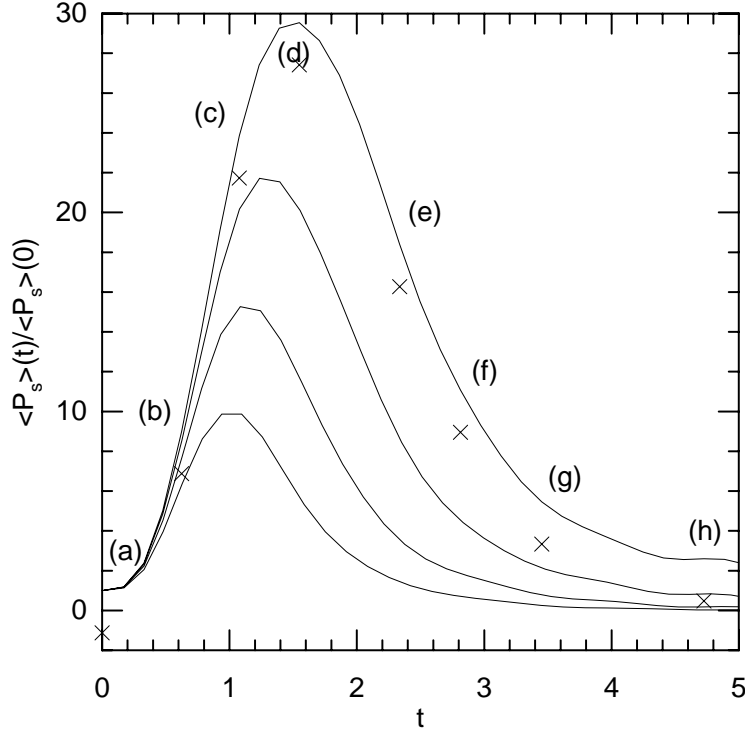


FIGURE 5. The growth of the volume average of the palinstrophy production for various initial microscale Reynolds numbers for the Gaussian case. ( $R_\lambda(0) = 2338, 1169, 585, 292$  from the top to the bottom.) The values are normalized by the initial value.

value of  $P_s$ . (The sampling times of the snapshots are marked on the curve for the largest Reynolds number in Fig. 5.)

At  $t = 0$  the ellipse is located with the longer axis vertical. Even though the initial stage of the development is similar to the compact case (Fig. 6a and 6b), clearly we can observe that (1) the filament is less stretched and (2) the core is more circular than the previous case (Fig. 6c). The circular core persists for a long time and the filament winds around it rather continuously in space and time (Fig. 6d ~ 6g). In Fig. 6h, however, some defects of the spirals are seen at the root in the core region. Disconnection of the filaments is observed at the root at the edge of the core where  $P_s$  takes negative values.

Figure 7 is the energy spectrum at  $t = 4.73$  (a) (the time corresponds to that for Fig. 6h), and at  $t = 7.77$  (b). Plots of  $k^3 E(k)$  together with  $k^{11/3} E(k)$  and  $k^4 E(k)$  are presented for comparison. At the earlier time leveling of the  $k^3$  compensated spectrum is observed, with fluctuations in the middle range of the wave number, around  $20 < k < 60$ . At the latter time, however, a normalization  $k^{11/3} E(k)$  by Gilbert (1988) and Moffatt (1990) which is based on the existence of spiral structures seems to work better.

Similarly to Fig. 4, Fig. 8 shows the average of palinstrophy production  $P(P_s|\omega)$  conditionally sampled from the equal magnitude set of vorticity at the times corresponding to Fig. 6a to 6g (i.e. at the marked positions in Fig 5).

Again we see that the palinstrophy production stays almost zero at zero vorticity (back ground) and at the maximum vorticity (in the core). Also the main peak shifts to the smaller vorticity. Contrarily to the previous case, however, the average shows clear oscillation (Fig. 8e-8h). It is almost certain that the oscillation is due to the spirals. The amplitude of the oscillation decreases except for the main peak (Fig. 8h) and we expect

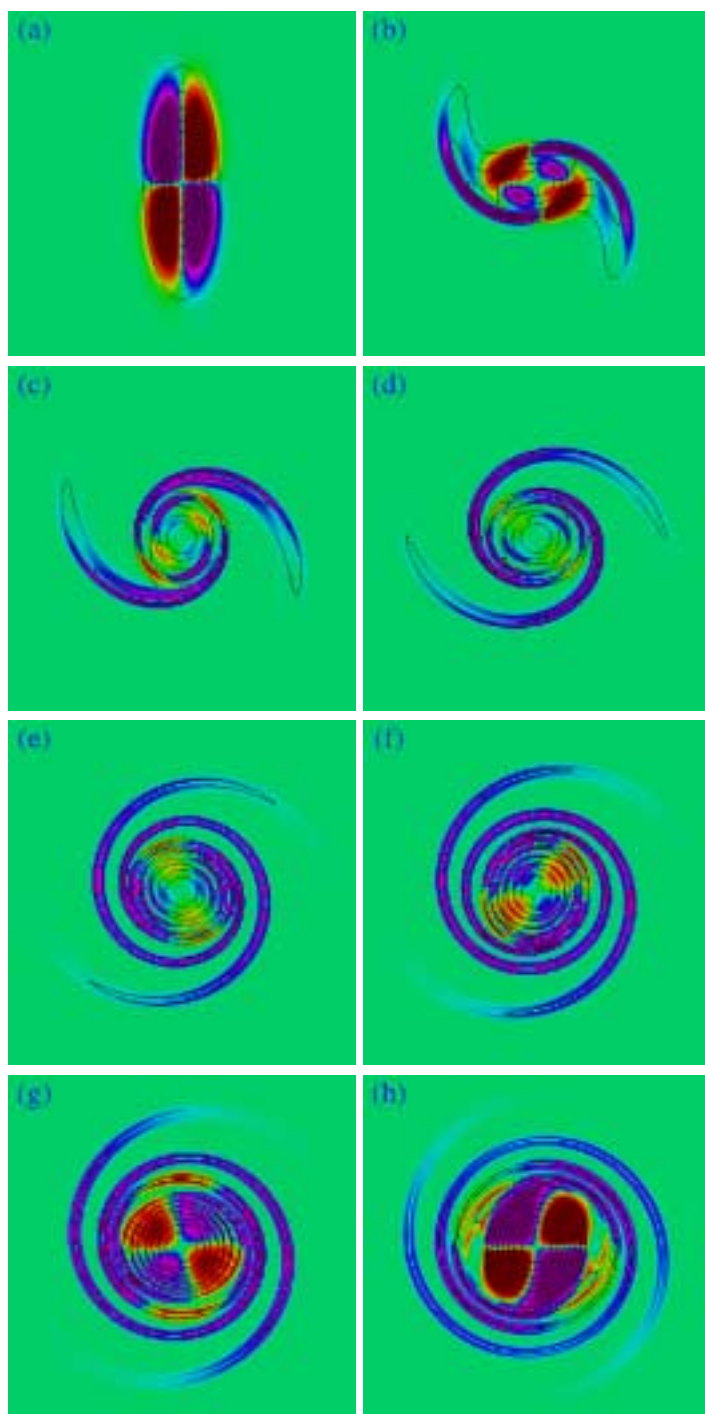


FIGURE 6. Snapshots of the equivorticity contour lines colored with the value of the palinstrophy production for Gaussian initial conditions. The data are sampled for the highest  $R_\lambda(0)$  case, and the sampling times are indicated by the cross marks with the labels on the plot in Fig. 5.

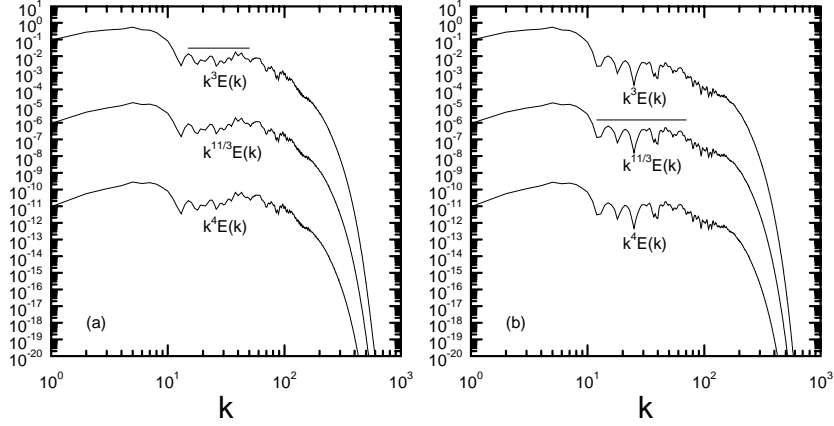


FIGURE 7. The compensated energy spectrum,  $k^3 E(k)$ ,  $k^{11/3} E(k)$  and  $k^4 E(k)$ , for the Gaussian initial condition (a)  $t = 4.73$  and (b)  $t = 7.77$ . The last two are shifted down by 5 decades each.

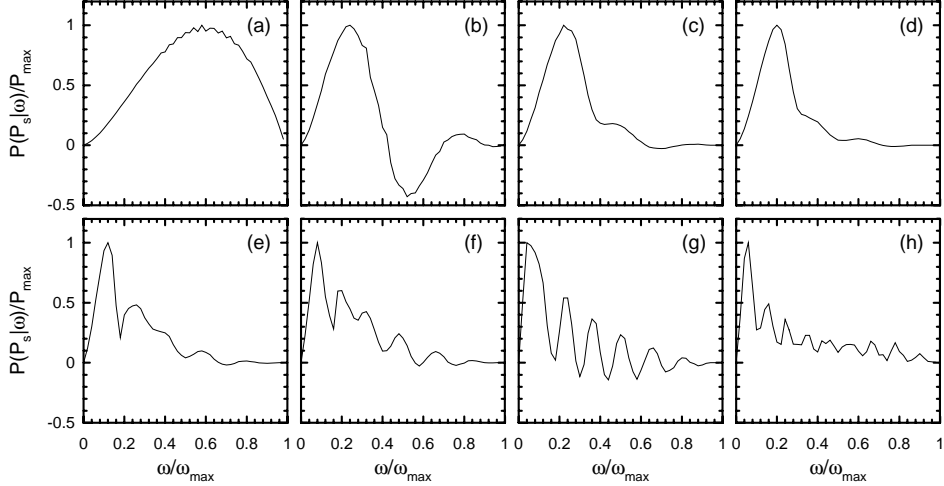


FIGURE 8. Conditional average of the palinstrophy production in terms of the magnitude of vorticity for the Gaussian case. The labels correspond to those in Fig. 5 and Fig. 6.

that only the main peak survives asymptotically as time goes on. The contrast seems interesting between the oscillatory behavior in space and the rather smooth development of the total palinstrophy in time.

#### 4. Discussion

Figure 9 shows a snapshot of vorticity contours (black: positive ; red: negative) from the pseudo-spectral simulation with a random Gaussian initial condition which is colored as before by the value of the palinstrophy production. The domain shown is the one-eighth center-cut of the total domain of  $2048^2$  grid points.

We see a number of elliptic vortices which have a quadrupole structure of the palinstrophy production just as a single elliptic vortex in the preceding section. The abundance of non-uniform elliptic vortices which carry very similar quadrupole structure to a single

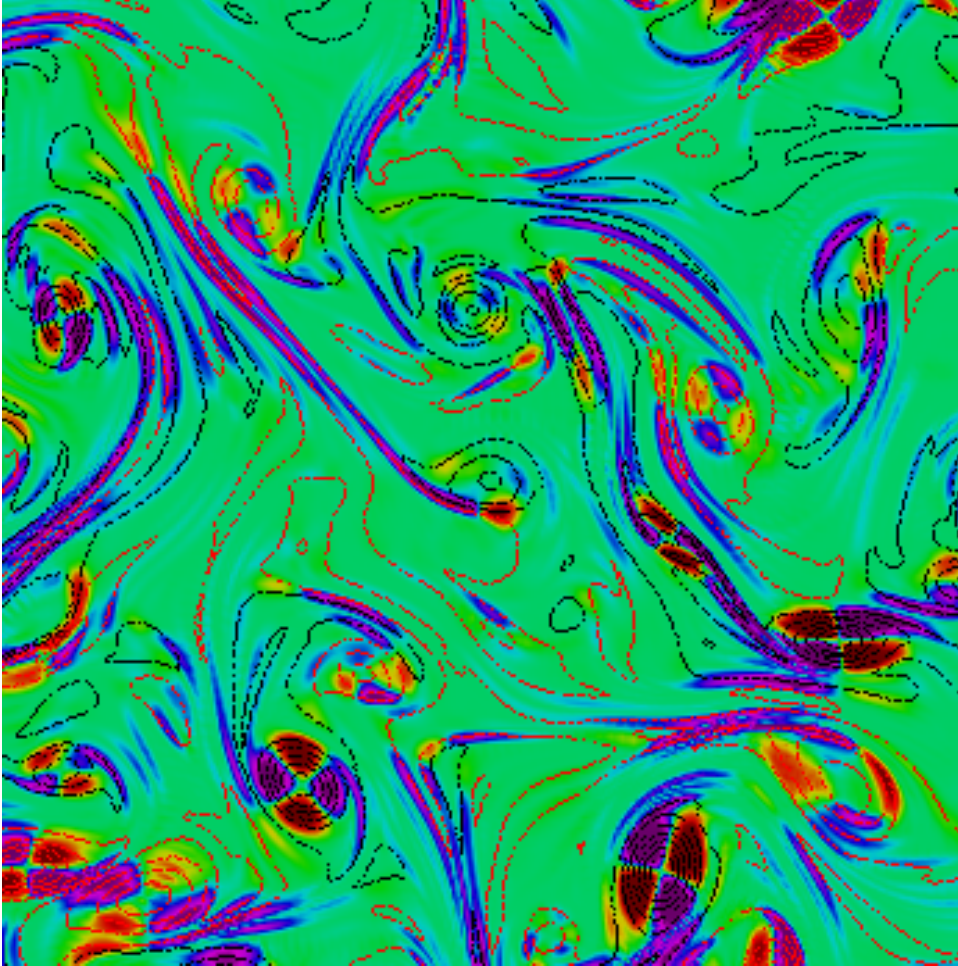


FIGURE 9. Snapshot of vorticity contours (black: positive ; red: negative) colored by the value of the palinstrophy production from the pseudo-spectral simulation with a random Gaussian initial condition.

elliptic vortex suggest the applicability of the present simplified theory to more general situations including turbulence.

One of the major differences for the random case is that the filaments ejected from elliptic vortices sometimes maintain strong palinstrophy production as well as vorticity due to the nonlinear interaction from other vortices and filaments in the background flow.

It is interesting to note that a non-uniform elliptic vortex in general has the quadrupole structure for palinstrophy production,  $P_s$ , and that the 2<sup>nd</sup> and 4<sup>th</sup> quadrants in a (positive) elliptic vortex are fated for positive stretching even without any effect of outer flows. Here we would like to repeat and summarize the scenario of the vorticity gradient enhancement and subsequent filament ejection. First, vorticity gradient enhancement by positive palinstrophy production results in overtaking of contour lines, which reminds us of the front (or the singularity) genesis in fluids. Perhaps due to incompressibility, the squash of the region is compensated by ejecting and stretching a vorticity filament from

the tip. The direction of stretching is determined as perpendicular to the maximum vorticity gradient. In the course of stretching, the region of positive palinstrophy production induces a pair to enhance the ejection of filament effectively.

The near final stage of 2D turbulence in a bounded domain is an interesting subject. From the previous study, the very final stage may be a vortex lattice with only one vortex in each fundamental cell (Matthaeus, *et al.* 1990). From the view point of palinstrophy production, a circular (or axisymmetric) vortex produces no palinstrophy, and is qualified as a steady state solution of the 2D Navier-Stokes equations. Perhaps shielding by the cloud of (weak) palinstrophy production maintains the circular shape of a vortex even in the earlier stage of development. †

It is still an open question how much can be said about the statistics of 2D turbulence in terms of the present theory on palinstrophy production. One way we can propose is (as we did in §2) to develop the stretching analysis in 2D turbulence and compare with 3D turbulence. The governing equation for stretching in 2D (eq. 2.5) has a similar form in 3D (eq. 2.6), but with the obvious difference that the former has an opposite sign for the production term compared to the latter. The essential difference in the stretching due to this sign difference should be studied in the future. In any event, however, we can say and have verified that non-uniform elliptic vortex is the simplest yet nontrivial building block to construct the theory which elucidates the stretching mechanism in 2D turbulence.

The authors are grateful to Arkady Tsinober and Rich Rotunno for valuable suggestions and encouragements, and Norman Zabusky for providing his reprints on two dimensional turbulence.

YK acknowledges the support by a Grant-in-Aid (08404006) for Scientific Research from the Ministry of Education, Science, and Culture of Japan.

NCAR is sponsored by the National Science Foundation.

#### REFERENCES

- BATCHELOR G. K. 1967 —it An introduction to Fluid Dynamics p.277, Cambridge.  
 BATCHELOR G. K. 1969 Computation of the energy spectrum in homogeneous two-dimensional turbulence. *Phys. Fluids supplement II*, pp.233–239.  
 DRITSCHEL, D.G. & ZABUSKY, N.J. 1996 On the nature of vortex interactions and models in unforced nearly-inviscid two-dimensional turbulence. *Phys. Fluids* **8**, 1252–1256.  
 DRITSCHEL, D.G. 1998 On the persistence of non-axisymmetric vortices in inviscid two-dimensional flows. *J. Fluid Mech.* **371**, 141–155.  
 GILBERT, A.D. 1988 Spiral structures and spectra in two-dimensional turbulence. *J. Fluid Mech.* **193**, 475–497.  
 HERRING, J.R., S. A. ORSZAG, R. H. KRAICHNAN, & D. G. FOX 1974 Decay of two-dimensional homogeneous turbulence. *J. Fluid Mech.* **66**, 417–444.  
 KRAICHNAN, R.H. 1967 Inertial ranges in two-dimensional turbulence. *Phys. Fluids* **10**, 1417–1423.  
 LOVE, A.E.H. 1893 On the stability of certain vortex motions. *Proc. London Math. Soc.* **25**, 18–42.  
 MATTHAEUS W.H., STRIBLING, W.T., MARTINEZ, D., OUGHTON, S. & MONTGOMERY, D. 1991 Selective decay and coherent vortices in two dimensional incompressible turbulence. *Phys. Rev. Lett.* **66**, 2731–2734.

† Recently, Dritschel (1998) pointed out a possibility of steady non-axisymmetric vortex. The existence of such solutions may be examined by the concept reported in this paper.

- MELANDER, M. V., MCWILLIAMS, J. C. & ZABUSKY, N.J. 1987 Axisymmetrization and vorticity-gradient intensification of an isolated two-dimensional vortex through filamentation. *J. Fluid Mech.* **178**, 137–159.
- MOFFATT, H. K. 1990?? Spiral structures in turbulent flows. Preprint of the lecture at the IMA Conference on 'Wavelets, Fractals, and Fourier Transforms: New Developments and New Applications', Cambridge, UK. 17–18 December.
- MOORE, D.W. & SAFFMAN, P.G. 1971 Structure of a line vortex in an imposed strain. *Aircraft wake turbulence* eds. Olsen, Goldberg, Rogers 339–54, Plenum.
- SAFFMAN, P.G. 1971 On the spectrum and decay of random two-dimensional vorticity distributions at large Reynolds number. *Stud. Appl. Maths.* **50**, 377.
- SAFFMAN, P.G. 1992 *Vortex dynamics*, Cambridge.
- TSINOBER, A., SHTILMAN, L. & VAISBURD, H. 1997 A study of properties of vortex stretching and enstrophy generation in numerical and laboratory turbulence. *Fluid Dynamics Research* **21**, 477–494.
- YAO, H.B., ZABUSKY, N.J. & DRITSHEL, D.G. 1995 High gradient phenomena in two-dimensional vortex interactions. *Phys. Fluids* **7**, 539–548.